Microplasma illumination enhancement in N+P co-ion implanted nanocrystalline diamond films

Salila Kumar Sethy[a,b], K. J. Sankaran[a,b,*], P. Gupta[c,d], J. P. Thomas[e], A. Dash[a], J. V. Kennedy[c,d], K. T. Leung[e], K. Haenen[f,g,*]

[a]*CSIR-Institute of Minerals and Materials Technology, Bhubaneswar 751013, India.*

[b]*Academy of Scientific and Innovative Research (AcSIR), CSIR-IMMT Campus, Ghaziabad 201002, India.*

[c]*National Isotope Centre, GNS Science, PO Box 30368, Lower Hutt 5010, New Zealand.*

[d]*The MacDiarmid Institute for Advanced Materials and Nanotechnology, School of Chemical and Physical Sciences, Victoria University of Wellington, PO Box 600, Wellington 6040, New Zealand.*

[e]*WATLab and Department of Chemistry, University of Waterloo, Waterloo, Ontario N2L3G1, Canada.*

[f]*Institute for Materials Research (IMO), Hasselt University, 3590 Diepenbeek, Belgium.*

[g]*IMOMEC, IMEC vzw, 3590 Diepenbeek, Belgium.*

Email address: kjsankaran@immt.res.in (K. J. Sankaran); and ken.haenen@uhasselt.be (K. Haenen).

Abstract

N and P co-ion implantation enhances the electrical conductivity of nanocrystalline diamond films to 6.9 S/cm and improves the microplasma illumination (MI) characteristics of the films to a low breakdown voltage of 340 V, large plasma current density of 6.3 mA/cm^2 (@ 510 V) with plasma life-

time stability of 10 h. N-ions induce nanographitic phases in the films and P-ions lower the resistance at the diamond-to-Si interface together promoting the conducting channels for effective electron transport, consequently attaining the improved MI properties of the films.

Keywords: nanocrystalline diamond; co-ion implantation; graphite; grain boundaries; electrical conductivity; microplasma illumination

---

1. Introduction

Microscale-dimensional microplasma is a low-temperature plasma, which has gained huge interest owing to its low price, handiness, and robustness in a broad spectrum of applications, such as plasma displays, materials synthesis, silicon etching, ultraviolet sources, spectroscopy of gases, and plasma medicine [1–3]. Though numerous technological applications of microplasma illumination (MI) devices have been advanced, the search for a proper cathode material is still on for improving the microplasma characteristics including the long-standing stability of micro-discharges. Cathode materials such as silicon, MgO, Al_2O_3, boron nitride, $BaTiO_3$, ZnO, carbon nanotubes, and graphene were employed in MI devices [4,5], however, due to their poor lifetime stability these cathodes cannot resist for a longer duration in a plasma environment. An important factor for the choice of cathode materials for MI devices is that the material should be efficient in generating abundant secondary electrons [i.e., large secondary electron emission (γ) coefficient], thereby increasing the stability of

micro-discharges.

Chemical vapor deposition (CVD) grown diamond film exhibits high thermal conductivity, good rigidity, high chemical inertness, low sputtering yield, and particularly, large γ coefficient, rendering it a suitable cathode material for MI devices [6,7]. The huge assurance that the diamond endures as an efficient cathode in the MI devices necessitates the films to be conductive. Electrically conducting diamond films were synthesized using appropriate dopants and impurities [8,9]. The induction of nanographitic phases in the grain boundaries of diamond films by incorporation of nitrogen increases the proportion of conduction paths, resulting in the enhancement of the electrical conductivity of the films [10]. However, the insulating nature of diamond grains confines the electrical conduction to the grainboundaries of diamond films, thus restraining the usage of nitrogen-incorporated diamond films in device applications. Alternatively, the phosphorus atom typically doped in substitutional positions of the diamond grains and forms a donor in both monocrystalline and polycrystalline diamond films [11,12].Nevertheless, a high growth temperature of around 800°C is necessitated to ionize these nitrogen and phosphorus dopants for generating good electrically conducting diamond films [9,10].

On the other hand, ion implantation is a feasible method to introduce the desired dopants into the diamond grains and grain boundaries to make the films electrically conductive [13,14]. With the aim of achieving electrically conducting grain boundaries (due to N ion implantation) between conducting diamond grains (due to P ion implantation), here we present an approach to co-ion implant N+P ions in nanocrystalline diamond (NCD) films for improving the electrical conductivity of NCD films for

the development of an effective cathode for MI devices. Interestingly, high electrical conductivity and enhanced MI characteristics, viz., low breakdown voltage (V_{bk}), large plasma current density (J_{PI}),and longer plasma lifetime stability (τ_{PI}) are achieved for the N+P co-ion implanted NCD (NCD_{N+P}) films. The bonding characteristics of NCD films are thoroughly investigated to understand themechanism of the enhancement of electrical conductivity and superior MI characteristics due to the co-ion implantation of N and P ions.

2. Materials and methods

2.1 Growth of NCD films

(100) silicon substrates (size 1 cm × 1 cm) were nucleated by spin-coating with 5 nm-sized detonation nanodiamond particles, which are dispersed in deionized water [8,10]. ASTeX 6500 series microwave plasma enhanced CVD system was used to grow NCD films on silicon substrates for a growth time of 1 h using CH_4(6%), H_2(89%), and N_2(5%) gas mixture of total flux 500 sccm. The microwave power and working pressure were set at 3000 W and 30 Torr, respectively, attaining a growth temperature of 650^{o}C (estimated using a single-color optical pyrometer). The as-grown NCD films were designated as NCD_{As}.

2.2 N and P co-ion implantation

The NCD_{As} films were then co-ion implanted at room temperature (RT) with N and P ions in a vacuum of ~10^{-6} Torr using a Penning ion source-based ion-implanter. Prior to co-ion implantation,

simulation studies (using the Monte Carlo program: T-Dyn)[15] were carried out to decide the energy, ion fluency, and order of implanted ions. First N ions were implanted on NCD films at an energy of 36 keVwith an ion fluency of 1×10^{15} ions/cm^2, followed by P ions of energy 72 keV with an ion fluency of 1×10^{15} ions/cm^2, respectively. The NCD films were also implanted with N and P ions separately forcomparison, which are designated as NCD_N (for nitrogen ion implanted NCD) and NCD_P (for phosphorus ion implanted NCD) films, respectively.

2.3 Materials characteristics

The surface morphology of the NCD films was observed using field emission scanning electron microscopy (FESEM; (Zeiss SUPRA55)). The depth profiles of the ion-implanted NCD films were performed in a time-of-flight secondary ion mass spectroscopy (TOF-SIMS; an ION-TOF 5 IONTOF GmbH) system. The measurement was carried out in the spectrometry mode (negative polarity) with an analyzer ion source of Bi+ ions (30 keV) and Cs ions (1 keV) used as the sputtering source. The analysis was performed with a cycling time of 200 µs for an analysis area of 150 × 150 µm^2 and a sputtering area of 350 × 350 µm^2. The electrical conductivity of the NCD films was measured using Hall effect measurements under the van der Pauw configuration. The bonding characteristics of these NCD_{N+P} films were thoroughly investigated using visible-Raman spectroscopy (Lab Raman HR800, Jobin Yvon; λ=532 nm) and X-ray photoelectron spectroscopy (XPS; Thermo-VG Scientific ESCALab 250microprobe) studies. The XPS analyses were carried out through CasaXPS software and

the peaks were fitted using the Gaussian curve fitting method.

2.4 Microplasma illumination studies

The MI device was fabricated using an indium tin oxide (ITO)-coated glass as anode and the NCD films as cathode. The anode and the cathode were separated by a 0.15 mm thick Teflon spacer. A microcavity was generated by a circular hole of diameter 3.0 mm on the spacer. The chamber was vacuumed with a base pressure of 0.1 mTorr and externally connected to a DC power supply through a 56 kΩ resistor. Prior to measurements, all the samples were heated at 200°C (1 h) to remove moisture on the surface of the samples in order to improve the reliability of the measurements. Ar gas at a flow rate of 10 sccm was channeled into the chamber. The DC voltage was increased linearly from 0 V to breakdown and then up to the maximum voltage of 600 V for all the devices (at room temperature). A source meter, Keithley 2470,was utilized to measure the plasma current at constant pressure with respect to the applied voltage. An USB microscope was utilized to view the plasma.

3. Results and discussion

Figure 1(a) displays the plan-view FESEM micrograph of NCD_{As} films, which reveals diamond grains of size 50–80 nm with roundish granular structure. It is to be noted that the addition of 5% N_2 in the CH_4/H_2 plasma effects in the reduction of diamond grain size and subsequent increase in the grain boundaries of the NCD films [16]. The thickness of NCD_{As} films is around 470 nm for a growth time of 1 h, which was estimated using cross-sectional FESEM [inset of Figure 1(a)]. The depth profiles

shown in Figure 1(b) suggest that the N ions uniformly spread into the NCD films, whereas the P ions donot spread into diamond films, which are localized on the diamond-Si interface because of the low solubility of phosphorus ions [17]. This depth profile approves that N and P ions have been implantedin the NCD films. The co-ion implantation does not damage the morphology of the NCD films (figurenot shown), which looks similar to the morphology of the NCD_{As} films as shown in Figure 1(a).

Curve (i), inset of Figure 2(a) demonstrates the RT electrical conductivity (σ) values of ion-implanted NCD films evaluated by the van der Pauw configured Hall measurement system. The negative Hall coefficient value indicates that electrons are the major charge carriers of NCD_{N+P} films. The NCD_{N+P} films show the highest electrical conductivity (σ) value of 6.9×10^{-2} S/cm [curve (i), Figure 2(a)] nevertheless the NCD films implanted only with N and P ions (NCD_N and NCD_P films) show low σ values of 5.8×10^{-5} S/cm and 1.9×10^{-5} S/cm, respectively. The obtained electrical conductivity of NCD_{N+P} films are comparable with the other ion-implanted diamond films tabulated in Table 1[18–24], which is a beneficial factor for electron emission device applications. Furthermore, the Hall measurements were accomplished at temperatures from RT to 573 K [Figure 2(b)]. All the films show an increasing trend of σ [Figure 2(b)] with an increase in temperatures. Particularly, the highest σ value of 6.9 S/cm at 573 K is achieved for the NCD_{N+P} films. The increase in the electrical conductivity with respect to temperature, thus reveals a thermally activated conduction mechanism[25]. Such highly electrically conducting NCD_{N+P} films can be suitable as cathodes for field electron emission devices such as MI devices.

The schematic diagram of the MI device utilizing NCD films as cathode is illustrated in Figure 3(a).The plasma photographs presented in Figure 3(b) determine the MI characteristics of the NCD_{N+P}

films employed as cathodes in the MI device. Comparably the NCD_{N+P} films as cathode triggered the plasmaat the lowest V_{bk} value of 340 V from other NCD films as cathodes in the MI device [Figure 3(b) (i)−(iv)].For all the NCD films, the brightness of the plasma illumination increases with an increase in applied voltage, however, the intensity of the plasma is higher for the NCD_{N+P} films at the applied voltage of 600 V. Moreover, the J_{PI} versus applied voltage (V) plotted in Figure 3(c) reveals that the NCD_{N+P} films show the lowest V_{bk} value of 340 V followed by NCD_N films (380 V), NCD_P films (430 V), and NCD_{As}films (470 V), respectively [curve (ii), Figure 2(a)]. The highest J_{PI} value of 6.3 mA/cm^2 at V_{bk} = 510 V is observed for NCD_{N+P} films [curve (iv), Figure 3(c)]. It is noticeable that the high electrical conductingNCD films (NCD_{N+P}) perform better as a cathode in MI devices. Besides, τ_{PI} of the NCD_{N+P} filmsis measured at a constant J_{PI} of 2.5 mA/cm^2 [inset of Figure 3(c)]. The NCD_{N+P} films attain the highest τ_{PI} of approximately 10 hours [curve (ii), inset of Figure 3(c)] as compared to the NCD_{As} films (approximately 6 hours). Remarkably, the MI characteristics of the NCD_{N+P} films as cathodes providesignificant enhancements as compared to other cathode materials in the MI devices described previously and are tabulated in Table 2 [26–36].

To elucidate how the NCD_{N+P} films attain higher electrical conductivity and enriched MI characteristics, the bonding characteristics of these films were thoroughly investigated using Raman spectroscopy and XPS studies. Raman spectroscopy is a substantial tool to examine the different carbon phases existing in diamond films. Figure 4(a) shows the visible-Raman spectra of the (i)

NCD_{As}, (ii) NCD_{P}, (iii) $NCD_{N,}$ and (iv) NCD_{N+P} films. The multi-peak Lorentzian fitting method was used to deconvolute the Raman peaks. Spectrum (i) of Figure 4(a) illustrates that the Raman spectrum ofthe NCD_{As} films, which comprises a peak at 1336 cm^{-1} corresponding to sp^3-bonded carbon (designated as "dia"), a D-band at ~1350 cm^{-1} (disordered carbon), a G-band at ~1580 cm^{-1} (graphite), a ν_1-band at ~1200 cm^{-1} (*trans*-polyacetylene phase, *t*-PA, seemingly positioned along the grain boundaries) [8]. The typical Γ_{2g} resonance peak at 1336 cm^{-1} for the diamond lattices is scarcely noticeable because the visible-Raman is highly sensitive to the sp^2- bonded carbon than the sp^3-bonded carbon [14].

Furthermore, curve (i) of Figure 4(b) reveals a decrease in the G band full-width half maximum (FWHM), and curve (ii) of Figure 4(b) shows the shifting of the G band to a higher wavenumber for the NCD_N and NCD_{N+P} films. These observations indicate the materialization of sp^2-graphitic content in the NCD films due to N and N+P ion implantations [34]. On the other hand, it is observed that the FWHM of the G band increases, and the G band shifts to a lower wavenumber of NCD_P films, which indicates that P-ion implantation induces the amorphization of NCD films [35,36]. Furthermore, curve (i) of Figure 4(c) displays the I_D/I_G values (ratios of the integrated intensities of the D and G lines) of 0.40, 0.35, 0.73, and 0.94 for the NCD_{As}, NCD_P, $NCD_{N,}$ and NCD_{N+P} films, respectively. This indicates that the NCD_{N+P} films contain abundant nanographitic phases and a decrease in the sp^3 content [37,38]. Curve (ii) of Figure 4(c) illustrates a decrease in the $I_{t\text{-}PA}/(I_D + I_G)$ ratio of the NCD films after ion

implantation, demonstrating that the *t*-PA content is reduced in the films. Particularly, the *t*-PA content in the NCD_P films is lower as compared to NCD_N and NCD_{N+P} films, indicating the induction of amorphization in NCD_P films because of P-ion implantation, as indicated in the earlier observations[32,33]. The G-band FWHM, G-peak position, I_D/I_G, and $I_{t\text{-}PA}/(I_D+I_G)$ values obtained from Raman spectra of NCD films are tabulated in Table 3.

The near-surface characteristics of NCD films after ion implantation were explored using XPS. The C1s photoemission spectra of the (i) NCD_{As}, (ii) NCD_P, (iii) NCD_N, and (IV) NCD_{N+P} films are revealed in Figure 5. The background was subtracted by Shirley's method [15] and the data were fitted with Lorentzian peaks to estimate the relative intensities of the sp^3 and sp^2 components of the NCD films,respectively (Table 3). In NCD_{As} films [spectrum (i) of Figure 5], sp^3 C–C bonding is the main with the peak intensity of 62.6% associated with the sp^2 C=C intensity of 37.4%. Spectrum (ii) of Figure 5 showsa decrease in the sp^3 C–C peak intensity of 56.4% and an increase in the sp^2 C=C peak intensity of 43.6%for NCD_P films. Moreover, the peak position of the C1s spectrum of NCD_P shifts to lower binding energies, which indicates the lowering of the surface resistivity, probably via the formation of amorphous carbon clusters.[39] For NCD_N films [spectrum (iii) of Figure 5], the sp^3 C–C peak intensity decreases further to 41.1% and the sp^2 C=C peak intensity increases further to 58.9%. After N+P co-ion implantation, the NCD_{N+P} films show the highest sp^2 C=C peak intensity of 60.7% with the sp^3 C–C peak intensity of 39.3% [spectrum (iv) of Figure 5], respectively. The increase in sp^2 content upon

N+P co-ion implantation is reliable with our Raman results (cf. Figure 4). On the basis of Raman and XPS investigations, it is perceived that co-ion implantation of N and P-ions in NCD films (NCD_{N+P}) induceshigh sp^2-graphitic content than those of NCD_N and NCD_P films, respectively, ensuing better electrical conductivity and enhanced MI characteristics of NCD_{N+P} films.

A good field electron emitter should supply sufficient electrons from the substrate material (the silicon) to the emitting material (the diamond) besides the low work function of the emitting material [18]. Therefore, to improve the efficiency of the supply of electrons, it is necessitated to be mutually optimized the electrical conductivity of diamond as well as the interface resistance between diamond and Si. These requests are simultaneously fulfilled by the co-ion implantation of N and P ions in the NCD films. As observed from SIMS [cf. Figure 1(b)] that the uniform distribution of the N-ions throughout the NCD films induces the formation of nanographites in the grain boundary phases and hence increases the electrical conductivity of the films [20]. On the other hand, due to the low solubility of P-ions, they were found to be localized at the interface region between diamond and Si [17], which lowers the resistivity of the interface layer. Restated, both the electrical conductivity of the bulk NCD films and NCD-to-Si interface were improved because of the N and P co-ion implantation, correspondingly. The electrons therefore can be transported easily through the interface region between diamond and Si and can transfer effortlessly through the conducting grain boundaries of the films to the emitting surface [28–34] and thus achieved superior MI characteristics viz. low V_{bk} and high J_{PI} for the NCD_{N+P} films. Moreover, the NCD films contain comparatively large diamond grains of size

50–80 nm with considerable thin grain boundaries. The nanographitic grain boundaries betweenthe large diamond grains can endure damage during plasma ion bombardment and thus, the NCD_{N+P} films proved better τ_{PI} than those of other ion-implanted diamond films [26–33].

4. Conclusions

In summary, improved electrical conductivity and superior MI characteristics are attained for NCD_{N+P} films. The uniform distribution of N-ions in the NCD films induces nanographites in the grain boundaries that advance the electrically conducting nature of the films. Besides, P-ions localized in the interface region between diamond and Si lower the resistance of the interface layer and enhance the electron transportation at the interface. Consequently, the better MI characteristics viz. a low V_{bk} of 340 V and a high J_{PI} of 6.3 mA/cm^2, in conjunction with a long τ_{PI} of 10 hours of conducting NCD_{N+P} film are achieved, which makes this film a potential cathode material for applications in high brightness plasma devices.

CRediT authorship contribution statement

Salila Kumar Sethy is responsible for methodology, data curation, writing the manuscript. K. J. Sankaran is responsible for conceptualization, funding acquisition, investigation, methodology, project administration, supervision, and writing the manuscript. P. Gupta is responsible for conceptualization and investigation. J. P. Thomas is responsible for investigation and data curation. A. Dash is

responsible for investigation and data curation. J. V. Kennedy is responsible for methodology. K. T. Leung is responsible for methodology and data curation. K. Haenen is responsible for conceptualization, methodology, and project administration.

Declaration of competing interest

The authors declare that they have no known competing financial interests or personal relationships that could have appeared to influence the work reported in this paper.

Acknowledgments

The authors like to thank the financial support of the Science and Engineering Research Board (SERB), India, CSIR-Institute of Minerals and Materials Technology, India via Research Projects GAP-336 and OLP-106, the Methusalem NANO network, and the Research Foundation – Flanders (FWO) via project G0D4920N, the Ministry of Business, Innovation and Employment, New Zealand under the research contract C05X1905 and the MacDiarmid Institute for Advanced Materials and Nanotechnology.

References

[1] W. H. Chiang, D. Mariotti, R. M. Sankaran, J. G. Eden, K. Ostrikov, Adv. Mater. 2020, 32, 1905508.

[2] Y. Fu, H. Wang, B. Zheng, P. Zhang, Q. H. Fan, X. Wang, J. P. Verboncoeur, Appl. Phys. Lett. 2021, 118, 174101.

[3] J. Cheng, W. Ding, Y. Zi, Y. Lu, L. Ji, F. Liu, C. Wu1, Z. L. Wang, Nat. Commun. 2018, 9, 3733.

[4] Q. Liu, Z. Yang, Y. Wang, G. Ding, Nano-Micro Lett. 2012, 4, 247−252.

[5] K. J. Sankaran, B. R. Huang, A. Saravanan, D. Manoharan, N. H. Tai, I. N. Lin, ACS Appl. Mater. Interfaces 2015, 7, 27078−27086.

[6] S. C. Lou, C. Chen, K. Y. Teng, C. Y. Tang, I. N. Lin, J. Vac. Sci. Technol. 2013, 31, 02B109.

[7] S. Kunuku, K. J. Sankaran, K. C. Leou, I. N. Lin, Mater. Res. Express 2017, 4, 025001.

[8] S. K. Sethy, M. Ficek, K. J. Sankaran, S. Sain, A. R Tripathy, S. Gupta, J. Ryl, S. S. Roy, N. H. Tai, and R. Bogdanowicz, ACS Appl. Mater. Interfaces 2021, 13, 55687−55699.

[9] N. Lambert, Z. Weiss, L. Klimsa, J. Kopecek, Z. Gedeonova, P. Hubik, V. Mortet, Diamond Relat. Mater. 2022, 125, 108964.

[10] K. J. Sankaran, C. J. Yeh, P. Y. Hsieh, P. Pobedinskas, S. Kunuku, K. C. Leou, N. H. Tai, I. N. Lin, K. Haenen, ACS Appl. Mater. Interfaces 2019, 11, 25388−25398.

[11] S. Choudhury, R. Golnak, C. Schulz, K. Lieutenant, N. Tranchant, J. C. Arnault, M. A. P. Thaury, F. Jomard, P. Knittel, T. Petit, Carbon 2021, 7, 28.

[12] W. Janssen, S. Turner, G. Sakr, F. Jomard, J. Barjon, G. Degutis, Y.-G. Lu, J. D'Haen, A. Hardy, M.K. Van Bael, J. Verbeeck, G. Van Tendeloo, K. Haenen, Phys. Status Solidi (RRL) 2014, 8/8, 705.

[13] D. Das, and M. S. R. Rao, RSC Adv. 2021, 11, 23686–23699.

[14] T. Chakraborty, K. J. Sankaran, S. Kunuku, R. Nongjai, K. Asokan, C.H. Chen, H. Niu, K. Haenen, Diamond Relat. Mater. 2021, 120, 108587.

[15] J. P. Biersack, S. Berg, C. Nender, Nucl. Instrum. Methods Phys. Res. B 1991, 59, 21.

[16] K. J. Sankaran, K. Srinivasu, C. J. Yeh, J. P. Thomas, S. Drijkoningen, P. Pobedinskas, B. Sundaravel, K. C. Leou, K. T. Leung, M. K. Van Bael, M. Schreck, I. N. Lin, K. Haenen, Appl. Phys. Lett. 2017, 110, 261602.

[17] E. S. Cho, B. G. Park, J. D. Lee, S. J. Kwon, J. Vac. Sci. Technol. B 2003, 21, 603.

[18] X. J. Hu, J. S. Ye, H. Hu, X. H. Chen, Y. G. Shen, Appl. Phys. Lett. 2011, 99, 131902.

[19] X. J. Hu, J. S. Ye, H. J. Liu, Y. G. Shen, X. H. Chen, H. Hu, J. Appl. Phys. 2011, 109, 053524.

[20] R. Arenal, P. Bruno, D. J. Miller, M. Bleuel, J. Lal, D. M. Gruen, Phys. Rev. B 2007, 75, 195431.

[21] K. J. Sankaran, H. C. Chen, B. Sundaravel, C. Y. Lee, N. H. Tai, I. N. Lin, Appl. Phys. Lett. 2013, 102, 061604.

[22] K. J. Sankaran, K. Panda, B. Sundaravel, N. H. Tai, I. N. Lin, J. Appl. Phys. 2014, 11, 063701.

[23] K. J. Sankaran, K. Panda, B. Sundaravel, N. H. Tai, I. N. Lin, J. Mater. Chem. C 2015, 3, 2632.

[24] K. J. Sankaran, K. Srinivasu, C. J. Yeh, J. P. Thomas, S. Drijkoningen, P. Pobedinskas, B. Sundaravel, K. C. Leou, K. T. Leung, M. K. Van Bael, M. Schreck, I. N. Lin, K. Haenen, Appl. Phys. Lett. 2017, 110, 261602.

[25] S. S. Gu, X. J. Hu, J. Appl. Phys. 2013, 114, 023506.

[26] K. J. Sankaran, K. Srinivasu, K. C. Leou, N. H. Tai, I. N. Lin, Appl. Phys. Lett. 2013, 103, 251601.

[27] K. J. Sankaran, T. H. Chang, S. K. Bikkarolla, S. S. Roy, P. Papakonstantinou, S. Drijkoningen, P. Pobedinskas, M. K. V. Bael, N. H. Tai, I. N. Lin, K. Haenen, RSC Adv. 2016, 6, 63178.

[28] K. J. Sankaran, M. Afsal, S. C. Lou, H. C. Chen, C. Y. Lee, L. J. Chen, N. H. Tai, I. N. Lin, Small 2013, 10, 179.

[29] K. J. Sankaran, M. Ficek, S. Kunuku, K. Panda, C. J. Yeh, J. Y. Park, M. Sawczak, P. P. Michalowski, C. K. Leou, R. Bogdanowicz, I. N. Lin, K. Haenen, Nanoscale 2018, 10, 1345.

[30] K. J. Sankaran, D. Q. Hoang, S. Korneychuk, S. Kunuku, J. P. Thomas, P. Pobedinskas, S.

Drijkoningen, M. K. V. Bael, J. D'Haen, J. Verbeeck, K. C. Leou, K. T. Leung, I. N. Lin, K. Haenen, RSC Adv. 2016, 6, 90338–90346.

[31] K. J. Sankaran, S. Kunuku, B. Sundaravel, P. Y. Hsieh, C. H. Chen, K. C. Leou, N. H. Tai, I. N. Lin, Nanoscale 2015, 7, 4377–4385.

[32] T. H. Chang, P. Y. Hsieh, S. Kunuku, S. C. Lou, D. Manoharan, K. C. Leou, I. N. Lin, N. H. Tai, ACS Appl. Mater. Interfaces 2015, 7, 27526–27538.

[33] K. J. Sankaran, M. Kicek, K. Panda, C. J. Yeh, M. Sawczak, J. Ryl, K. C. Leou, J. Y. Park, I. N. Lin, R. Bogdanowicz, K. Haenen, ACS Appl. Mater. Interfaces 2019, 11, 48612–48623.

[34] H. Tsai, D. B. Bogy, J. Vac. Sci. Technol. 1987, 5, 3287.

[35] S. C. Lin, C. J. Yeh, C.L. Dong, H. Niu, K. C. Leou, I. N. Lin, Diamond Relat. Mater. 2015, 54, 47–54.

[36] D. Das, M. S. R. Rao, Diamond Relat. Mater. 2022, 128, 109212.

[37] A. C. Ferrari, J. Robertson, Phys. Rev. B: Condens. Matter Mater. Phys. 2000, 61, 14095.

[38] A. Ilie, A. C. Ferrari, T. Yagi, S. E. Rodil, J. Robertson, E. Barborini, P. Milani, J. Appl. Phys. 2001, 90, 2024.

[39] P. T. Joseph, N. H. Tai, Chi-Young Lee, H. Niu, W. F. Pong, and I. N. Lin. J. Appl. Phys. 2008, 103, 043720.

Table 1. Comparison between the electrical conductivity of NCD_{N+P} films and other ion-implanted diamond films.

Materials	Electrical conductivity (S/cm)
P-ion implanted UNCD[18]	0.09
O-ion implanted UNCD[19]	33.3
N-ion implanted UNCD[20]	---
Au-ion implanted UNCD[21]	185
Cu-ion implanted UNCD[22]	95.0
Pt-ion implanted UNCD[23]	94.0
Li-ion implanted NCD[24]	11.0
NCD_{N+P}[this study]	6.9×10^{-2}

UNCD=ultrananocrystalline diamond

Table 2. Comparison between the MI characteristics of NCD_{N+P} films and other cathode materials.

Materials	V_{bk} (V)	J_{PI} (mA/cm^2)	τ_{PI}
Carbon nanotubes[26]	320	6.1 @ 510 V	190 min
Graphene nanoflakes[27]	400	3.3 @ 570 V	4 min
Diamond-graphene nanoflakes[28]	380	3.8 @ 570 V	21 min
Graphite[29]	220	2.6 @ 350 V	21 min
ZnO nanorods[30]	190	3.0 @ 300 V	---
UNCD-ZnO nanorods[31]	160	3.97 @ 300 V	107 min
MLG-BDD hybrid nanowalls[32]	330	6.0 @ 510 V	358 min
hBN-diamond nanorods[33]	350	1.04 @ 540 V	29 min
Gold-UNCD hybrids[34]	0.37	3.0 @ 520 V	7.12 h
Nitrogen-doped diamond films/CNTs[35]	0.36	1.88 @ 550 V	218 min
BNCD-CNS hybrids[36]	0.27	16.2 @ 500 V	545 min
NCD_{N+P} films[present study]	340	6.3 @ 510 V	10 h

V_{bk}=breakdown voltage; J_{PI}=MI current density; τ_{PI}= MI life-time stability; MLG=multilayered graphene; BDD=boron doped diamond; hBN=hexagonal boron nitride; CNTs=carbon nanotubes; CNS=carbon nanospines

Table 3. The G-band FWHM, G-peak position, I_D/I_G, and $I_{t\text{-}PA}/(I_D+I_G)$ values obtained from the Raman spectra of NCD films and the percentage of sp^3 and sp^2 bonding, as well as the peak positions of the XPS spectra of the NCD films.

Samples	Raman spectroscopy				XPS			
	G-FWHM (cm^{-1})	G-peak position (cm^{-1})	I_D/I_G	$I_{t\text{-}PA}/(I_D+I_G)$	sp^3 peak position (eV)	sp^2 peak position (eV)	sp^3 (%)	sp^2 (%)
NCD_{As}	124.3	1580.4	0.4	0.26	285.7	285.0	62.6	37.4
NCD_P	177.7	1580.4	0.25	0.24	285.3	284.7	56.4	43.6
NCD_N	129.1	1582.2	0.23	0.19	285.9	285.2	41.1	58.9
NCD_{N+P}	141.2	1582.9	0.18	0.18	285.8	285.2	39.3	60.7

Figure captions

Figure 1. (a) The plan-view FESEM micrograph of NCD_{As} surfaces with the inset shows the cross-sectional FESEM micrograph of NCD_{As} films. (b) shows the SIMS depth profiles of C, N, P, and Si species in NCD_{N+P} films.

Figure 2. (a) The room temperature electrical conductivity obtained from Hall effect measurement studies [curve (i)] and the breakdown voltage [curve (ii)] obtained from MI studies of the ion-implanted NCD films, respectively. (b) Temperature-dependent electrical conductivity for the (i) NCD_{As}, (ii) NCD_{P}, (iii) NCD_{N}, and (iv) NCD_{N+P} films, respectively.

Figure 3. (a) Schematic representation of microplasma illumination device. (b) Microplasma illuminationcharacteristics for the microplasma devices utilizing (i) NCD_{As}, (ii) NCD_{P}, (iii) NCD_{N}, and (iv) NCD_{N+P}films as cathodes. (c) Microplasma illumination current density (J_{PI}) as a function of applied voltage

(V) of (i) NCD_{As}, (ii) NCD_{P}, (iii) NCD_{N}, and (iv) NCD_{N+P} films as cathodes. The inset of (c) shows the microplasma illumination lifetime stability measurements of (i) NCD_{As} and (ii) NCD_{N+P} films measured at a constant J_{PI} =2.5 mA/cm^2.

Figure 4. (a) Visible-Raman spectra (λ=532 nm) of (i) NCD_{As}, (ii) NCD_{P}, (iii) NCD_{N}, and (iv) NCD_{N+P} films. (b) Variation in G-band FWHM [curve (i)] and G-peak position [curve (ii)] of the ion-implanted

NCD films. (c) Variation in I_D/I_G [curve (i)] and $I_{t\text{-}PA}/(I_D+I_G)$ [curve (ii)] of the ion-implanted NCD films.

Figure 5. The deconvoluted C1s XPS spectra of (i) NCD_{As}, (ii) NCD_P, (iii) NCD_N, and (iv) NCD_{N+P} films.

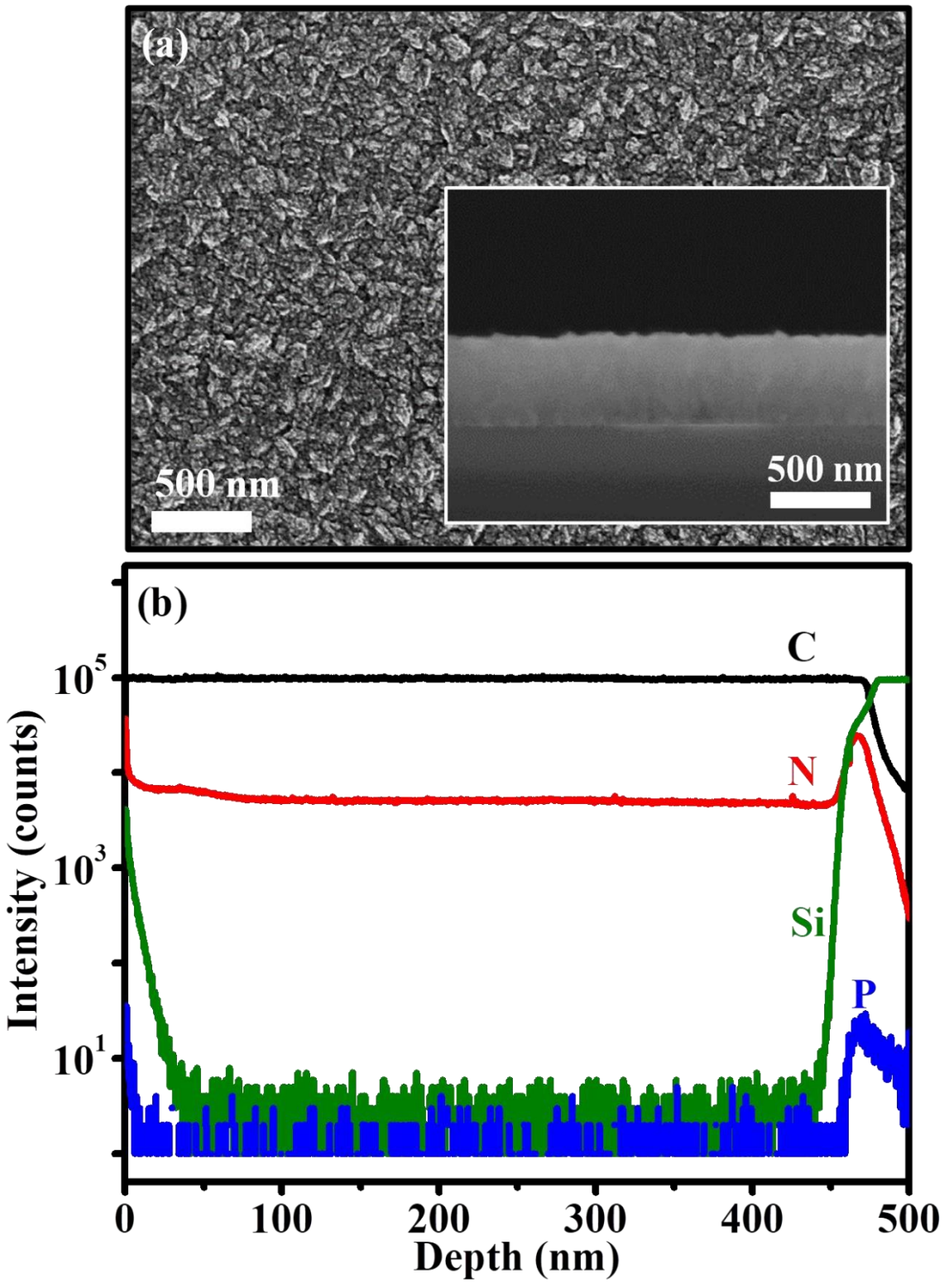
(a)
500 nm
500 nm
(b)
C
N
Si
P
Intensity (counts)
10^5
10^3
10^1
0
100
200
300
400
500
Depth (nm)

Figure 1.

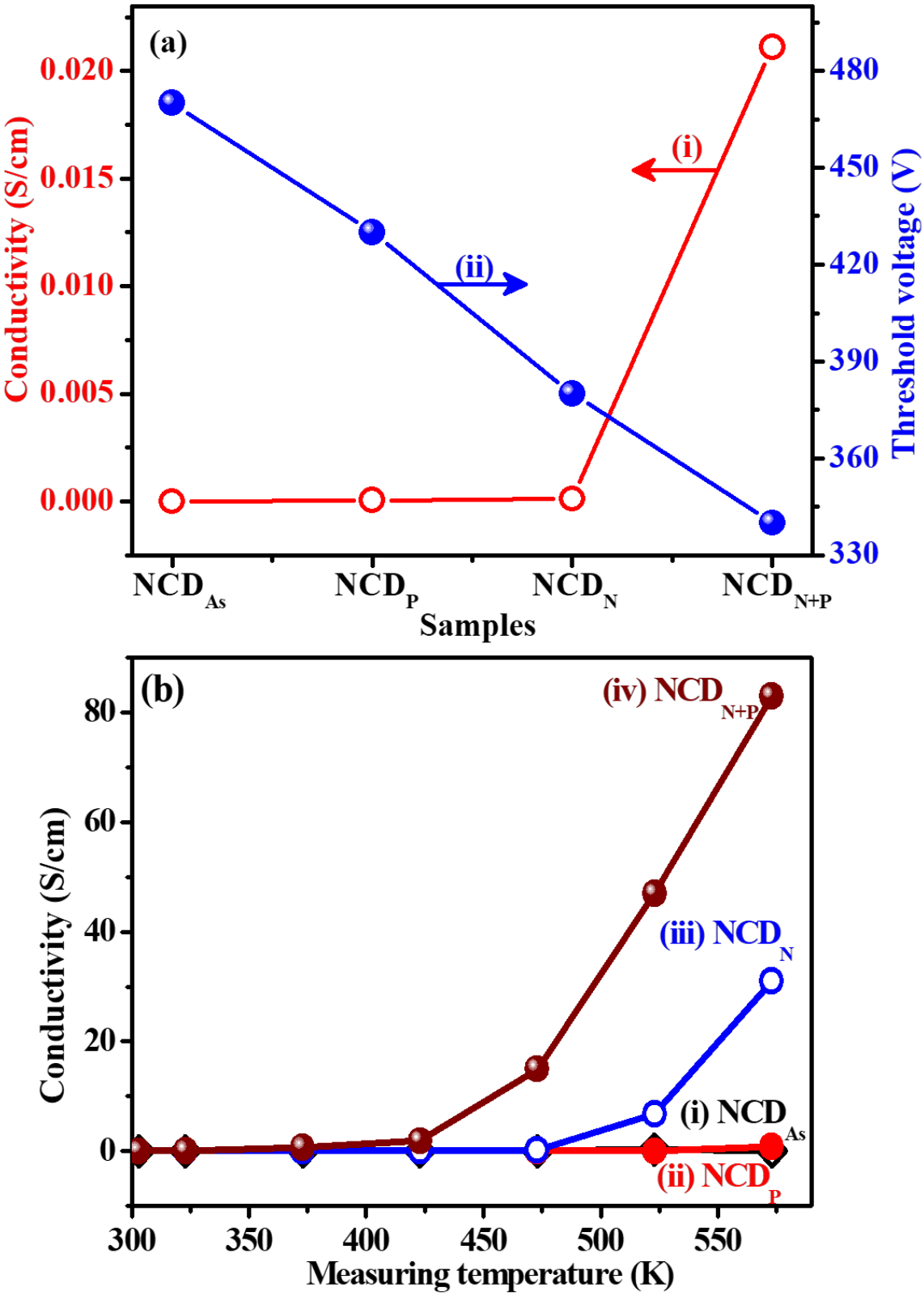
(a)
Conductivity (S/cm)
0.020
0.015
0.010
0.005
0.000
Threshold voltage (V)
480
450
420
390
360
330
(i)
(ii)
NCD As
NCD P
NCD N
NCD N+P
Samples
(b)
(iv) NCD N+P
(iii) NCD N
(i) NCD As
(ii) NCD P
Conductivity (S/cm)
80
60
40
20
0
300
350
400
450
500
550
Measuring temperature (K)

Figure 2.

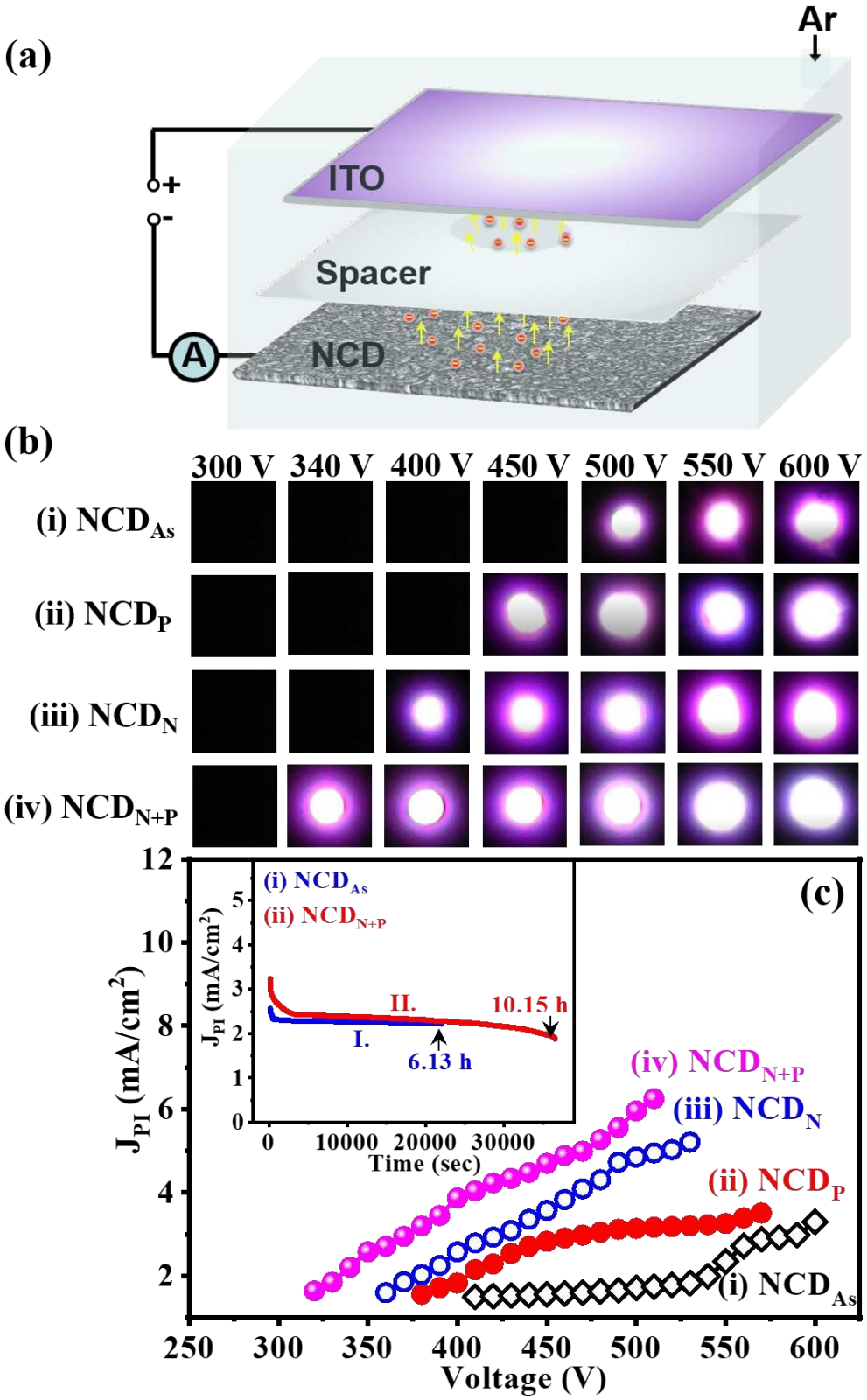
(a)
Ar
ITO
Spacer
NCD
+
-
A
(b)
300 V
340 V
400 V
450 V
500 V
550 V
600 V
(i) NCD$_{As}$
(ii) NCD$_{P}$
(iii) NCD$_{N}$
(iv) NCD$_{N+P}$
(c)
J_{PI} (mA/cm^2)
Voltage (V)
(i) NCD$_{As}$
(ii) NCD$_{N+P}$
II.
10.15 h
I.
6.13 h
Time (sec)
(iv) NCD$_{N+P}$
(iii) NCD$_{N}$
(ii) NCD$_{P}$
(i) NCD$_{As}$

Figure 3.

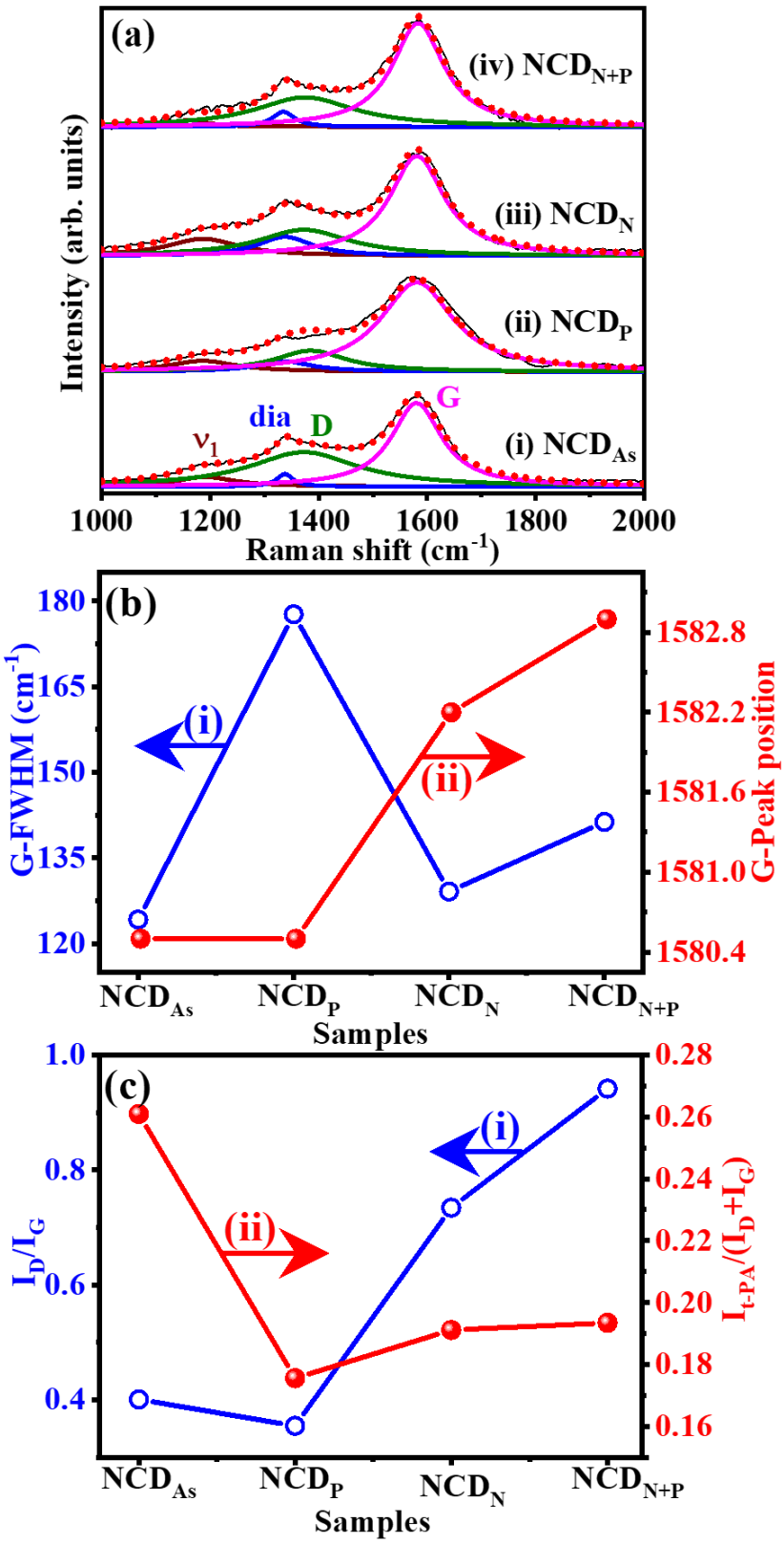
(a)
(iv) NCD$_{N+P}$
(iii) NCD$_N$
(ii) NCD$_P$
(i) NCD$_{As}$
dia
D
G
ν_1
Intensity (arb. units)
1000
1200
1400
1600
1800
2000
Raman shift (cm^{-1})
(b)
(i)
(ii)
G-FWHM (cm^{-1})
G-Peak position
180
165
150
135
120
1582.8
1582.2
1581.6
1581.0
1580.4
NCD$_{As}$
NCD$_P$
NCD$_N$
NCD$_{N+P}$
Samples
(c)
(i)
(ii)
I_D/I_G
$I_{t\text{-}PA}/(I_D+I_G)$
1.0
0.8
0.6
0.4
0.28
0.26
0.24
0.22
0.20
0.18
0.16
NCD$_{As}$
NCD$_P$
NCD$_N$
NCD$_{N+P}$
Samples

Figure 4.

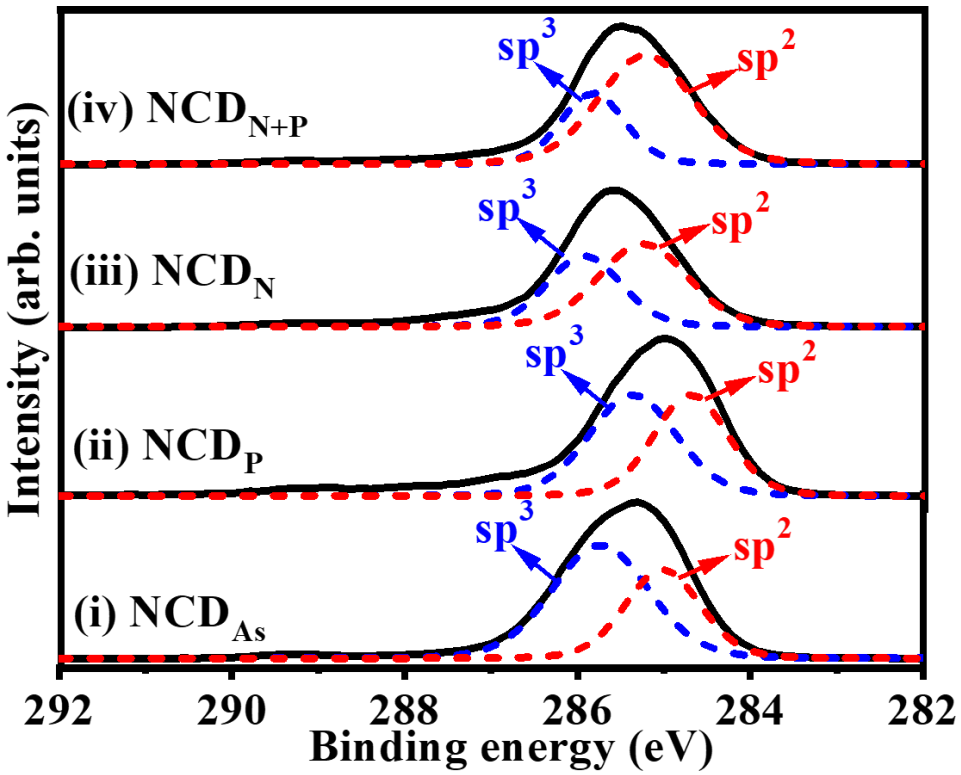
(iv) NCD$_{N+P}$
(iii) NCD$_{N}$
(ii) NCD$_{P}$
(i) NCD$_{As}$
sp^3
sp^2
Intensity (arb. units)
292
290
288
286
284
282
Binding energy (eV)

Figure 5.